4. PHOTOREFRACTIVE OPTICS

4.1 Introduction

When laser light passes through a turbulent flow, it is distorted by the density (refractive index) perturbations that are present. Although this phenomenon adversely affects the propagation of laser beams over long distances through turbulent media such as the atmosphere, it can be used to study turbulence since the perturbations of the laser beam contain information about the turbulence. Most laboratory experiments have small path lengths through the turbulent flow, so the perturbations are often quite small. This makes their detection and analysis difficult in the presence of the large, unperturbed portion of the laser beam.

Over the past few years several authors have investigated the application of nonlinear photorefractive materials (e.g., Pepper et al., 1990) to turbulence measurements, by separating the perturbations from the remainder of the beam. Robey (1990) and Robey et al. (1990) demonstrated application of the photorefractive effect by using barium titanate ($BaTiO_3$) as an optical filter in a turbulent channel flow experiment.

We had previously investigated the use of $BaTiO_3$ as a high-pass temporal filter for measurement of dynamic flow fields (O'Hern et al., 1991). Barium titanate is a photorefractive crystal which can be used to generate a standing-wave Bragg grating, i.e., a self-referenced real-time hologram of an incident coherent optical wavefront (Albrecht et al., 1990). The grating has the property that it scatters, or "fans" most of the incident radiation away from the optical axis. Because the grating formation has a time dependence, dynamic components of the incident wavefront will not be scattered out of the beam, while static components will be. In this way, the crystal acts as a temporal high-pass filter. In a turbulence experiment, the steady unperturbed laser beam is fanned away, so only the perturbed signal (containing the turbulence information) is transmitted and recorded for analysis. These effects have been previously demonstrated (Robey, 1990, Robey et al., 1990, O'Hern et al., 1991, and Papamoschou et al., 1993). The goal of the present work was to better quantify, calibrate, and demonstrate the technique.

This work has highlighted the capability of $BaTiO_3$ as a significant visualizer of turbulent vs. steady-state flow. However, we have identified two potentially significant limitations in that (1) it visualizes refractive index gradients, not absolute phase change, as desired and as reported in at least one reference, and (2) it appears to visualize refractive index gradients differently depending upon their orientation relative to the crystal fanning orientation.

We demonstrated that the $BaTiO_3$ photorefractive effect visualizes wavefront gradients, but not absolute phase variations in an optical field. It had been desired that the effect could be used as a single-beam self-referencing interferometer, in which the visualized flow would represent changes in optical phase, not wavefront slopes. Indeed a paper by Siahmakoun and Harrer (1993) claims that absolute dynamic phase shifts are detected by the effect. We have produced an experiment

which we believe refutes the published claim and demonstrates that changes in wavefront *slopes*, and not absolute dynamic phase shifts, are visualized.

We also performed a number of experiments to determine the effects of optical configuration (fanning orientation and edge orientation) on the image filtered by the $BaTiO_3$. Sensitivity of the photorefractive technique to orientation of the fanning direction of the crystal was demonstrated. The implication is that $BaTiO_3$ is sensitive to optical disturbances in one preferred gradient direction only, but does not visualize disturbances isotropically. Isotropic visualization is needed for unbiased measurement of turbulent flow fields. Furthermore, we raise concerns about whether a one-to-one correspondence can be established between a flow field and its visualized image due to mixing of the wavefront within a $BaTiO_3$ crystal.

4.2 Experimental Investigations

In this program we have attempted to demonstrate the use of a photorefractive crystal as a visualizer of optically refractive turbulent flow. We had also expected to draw quantitative data from the visualization, but this objective was not met for the reasons detailed below. There are two basic modes of operation using this technique. The first involves direct measurement of the turbulent power spectrum, while the second is a photorefractive schlieren. In both techniques, the $BaTiO_3$ crystal scatters out (fans away) all wavefront components which are static to within some time scale, allowing only the fluctuating turbulent flow component to transmit through the remainder of the optical system.

We have demonstrated the operation of $BaTiO_3$ using a cubic crystal with the faces cut at 45 degrees to the crystal "C" axis. Prior work (O'Hern et al., 1991) used crystals with the face cut normal to the "C" axis, which required tilting the crystal at a 45 degree angle relative to the input laser beam in order to observe the photorefractive effect. The tilt generated considerable astigmatism in converging wavefronts. Our current arrangement minimizes this effect.

4.3 Experimental Results

4.3.1. Turbulent Power Spectral Density Measurements

The power spectral density (PSD) diagnostic depends upon the property that a lens forms the two-dimensional Fourier power spectrum of an optical disturbance field at the lens focal plane. In the Fourier plane, one can then view the spatial frequency distribution of the optical disturbances. One of the problems with viewing the Fourier plane is that the nonzero spatial frequency components are usually weak and therefore dwarfed by the intensity of the zero spatial frequency (DC) component. By including the $BaTiO_3$ crystal into the beam path, the DC component of the beam is removed by fanning away from the optical axis, and the higher spatial frequency components can be better observed (Robey, 1990, Robey et al., 1990).

The experimental arrangement for the PSD setup is shown in Fig. 4.1. A Spectra-Physics 165 argon-ion laser operating at 514.5 nm was used as the optical source. The polarization of the laser was oriented in a vertical plane. The laser beam was expanded to 50 mm in diameter and directed through a flow cell where refractive disturbances were introduced. The optical configuration was modeled on ZEMAX, an optical design program, to establish that the design was capable of high quality optical imaging. The beam was directed into a 500 mm focal length doublet which then focused the beam to a point image. This plane constituted the "Fourier" plane, i.e., where the optical Fourier transform of the flow disturbance is formed. The $BaTiO_3$ crystal was positioned at this location with an orientation such that the resulting fanning was in the vertical direction. The transmitted light was expanded into a 125 mm focal length triplet relay lens which then directed the beam to a 1/2" Pulnix model TM745 charge-coupled device (CCD) based video camera. The camera was positioned at the image Fourier plane. Between the relay lens and the CCD camera neutral density filters could be positioned to attenuate the beam as needed. The video camera was coupled to an Imaging Technology VFG 100 frame grabber installed in a 386-based PC. The frame grabber permitted real-time observation of the CCD image, or up to four video frames to be captured in succession and stored in memory.

We demonstrated power spectrum measurements using a cold jet directed across the test section region. Fig. 4.2 illustrates the result. For the static case (regions of uniform density), the beam becomes nearly invisible, while in the dynamic case (regions of large density gradient), the power spectral density distribution becomes visible. In instances where we removed the photorefractive crystal from the optical train, the image of the power spectral density is swamped by the DC component of the signal. A static stray reflection is evident in all photos.

We attempted to calibrate the system for quantitative measurement of the PSD but quickly ran into difficulties. The PSD is actually a complicated relationship between the magnitude and spatial scale length of the phase disturbances (Papamoschou et al., 1993). Measuring the spatial scale of the disturbance would be straightforward since the width of the PSD is proportional to the maximum spatial frequency of the turbulent scale length. However, the Fourier transform is not a one-to-one relationship in phase because the phase term is a complex exponential. These PSD experiments emphasized that the major challenge remains quantification and calibration of the PSD image such that turbulence information can be extracted in order to evaluate the structures existing in the flowfield.

4.3.2. Temporal Schlieren Visualization

The temporal schlieren method, like the classical schlieren technique, visualizes spatial variations in the flow as an intensity variation in the schlieren image. In a typical implementation, a lens is used to image the flow field, which is illuminated by a collimated coherent laser wavefront, onto an image plane. At the focal (Fourier) plane of the lens, which lies between the lens and the image plane, the classical schlieren method uses a knife edge or slit to block optical gradients of specific values (Merzkirch, 1987). Spatial gradients in the flow field then appear as specific regions of light and dark, regardless of temporal history. A high quality wavefront must be transmitted through the

system with no temporal disturbance in order to present a nominal dark field view of the flow field. With the $BaTiO_3$ method, the crystal replaces the knife edge. Instead of blocking out gradients of a specific slope, the crystal scatters out all wavefront components which are static to within some time scale. Then, at the image plane, only the fluctuating turbulent flow components are viewed, even if large static optical disturbances are present. This yields, in effect, a dynamic, real-time holographic schlieren system.

The setup is shown in Fig. 4.3. The only difference between this configuration and the PSD configuration is that the CCD camera is positioned at a point where the phase disturbance plane is imaged. The visualized turbulent flow is shown in Fig. 4.4. In this example flowing CO_2 gas from a nozzle is visualized. The illustration shows how the visualized image flow can be combined with image processing to subtract out the background which was not completely extinguished by the crystal. Not shown is the image produced with no crystal present. In this case, the turbulent flow could not be visualized at all. Additional examples of photorefractive schlieren images are shown in O'Hern et al., 1991.

We demonstrate that the crystal is sensitive to dynamic effects only, and not static refractive effects in Fig. 4.5. In this instance, a phase object consisting of a heated soldering iron is placed in the field of view. When the soldering iron is allowed to generate a laminar heat flow in the surrounding air as in (A), the phase disturbance is invisible, but when the air is disturbed, as by introducing a slight cross current (B), the vertical stream because visible. View (C) is an image of image (A) subtracted from image (B) using image processing.

4.3.3. Orientation Effects on Flow Visualization

A number of experiments were conducted to determine the effects of fanning orientation and edge orientation on the image produced by the $BaTiO_3$ technique. The sensitivity of the photorefractive technique to orientation of the fanning direction of the crystal was initially noticed when a compressed-gas jet was directed horizontally then vertically with the same optical setup (Fig. 4.6). While the horizontal jet imaged strongly through the crystal, vertical venting of the jet produced very little dynamic response within the crystal. This directionality effectively introduces a bias into the image of any particular flow because the crystal will preferentially image gradients in a direction perpendicular to the fanning direction of the steady part of the optical signal. The strength of the directional sensitivity was quantified by comparing gray scale histograms for the images of the jet oriented horizontal and vertical, yielding significantly different distributions (Fig. 4.6C).

We repeated the demonstration with a well-controlled helium jet flow field. Figure 4.7 illustrates the effect. A low-pressure (5 psi) jet flow was directed across the test section perpendicular and parallel to the fanning direction. The perpendicular flow was visualized at a significantly brighter intensity than the parallel flow. Since the gradients in a flow are significantly greater in the direction perpendicular to the flow direction, we concluded that the photorefractive visualization is most sensitive to gradients in the fanning direction. The conclusion is that, like classical schlieren techniques, the photorefractive technique is sensitive to gradients in one orientation only.

4.3.4. Sensitivity to Wavefront vs. Slope Disturbances

We have demonstrated that the $BaTiO_3$ photorefractive effect visualizes wavefront gradients, but not absolute phase variations in an optical field. It had been desired that the effect could be used as a single beam self-referencing interferometer, in which the visualized flow would represent changes in optical phase, not wavefront slopes. Siahmakoun and Harrer (1993) claim that absolute dynamic phase shifts are detected by the photorefractive effect. We believe the following demonstration refutes the published claim by showing that changes in wavefront slopes, and not absolute dynamic phase shifts, are visualized. We contend that Siahmakoun and Harrer observed an effect due to changes in the polarization state of light due to birefringence, and not due to absolute phase change. In our experiment, we arranged two mirrors which share the aperture illuminated by the collimated beam (Fig. 4.8). One mirror was attached to a PZT translator driven by a ramped high voltage signal. This drove the mirror axially in "piston" through several waves of optical path change. The other mirror was held stationary. Were the crystal sensitive to absolute dynamic phase changes, one would observe in the image plane a modulated intensity across the aperture of the moving mirror, and no modulation in the image of the static mirror. In fact we observed no significant modulation in either mirror (Fig. 4.9), nor were there any substantial differences in images if one or another beam was blocked either before or after the crystal. However, we could observe some stray moving interference fringes, probably due to scattered light off of various surfaces in the crystal. Figure 4.10 illustrates that the extent to which extraneous temporally modulated fringes were observed was a function of how much overlap existed between the two beams inside the crystal. Beams overlapping within the crystal exhibit considerably more temporally modulated fringes than outside the crystal. This phenomenon alone is an indicator that the $BaTiO_3$ crystal as a flow visualizer is a complex effect and may be difficult to refine as a quantitative diagnostic.

4.3.5. Effect of Apertures

Obscurations placed across the object field contributed an extraneous glow at edges of the aperture. The observed glow was strongly dependent upon the orientation of the diffractive edge relative to the fan direction within the crystal and to the power of the incident beam entering the crystal. If a diffracting edge lay parallel to the fan direction, the effect was weak or nonexistent (Fig. 4.11). However, an edge perpendicular to the fan direction appeared to glow strongly, with an intensity dependent upon how much of the aperture was blocked (Fig. 4.12). This is additional evidence that there is an orientation effect associated with the $BaTiO_3$ techniques.

4.3.6. Temporal Transmission Measurements

The temporal crystal fanning response is highly dependent upon incident optical power density levels within the crystal. It is also dependent upon the residual grating remaining in the crystal from previously recordings. This effect made it difficult to characterize the crystal temporal bandpass

response, i.e., the $BaTiO_3$ temporal filter "settings." We did find that by repeatedly erasing the previously recorded Bragg grating with an incandescent, incoherent light source, we could obtain repeatable temporal extinction profiles which were dependent upon the length of the erasure light exposure. Figure 4.13 shows relative crystal extinction vs. time after a poling operation of the specified duration on a crystal which had achieved maximum extinction on a prior exposure. The time dependence of extinction appears to be approximately a negative exponential whose initial transmission is a function of the initial poling time. The peak transmission vs. poling time is replotted in Fig. 4.14, and can be seen to be approximately logarithmic in behavior.

4.4 Photorefractive PIV

Traditional PIV data analysis (see Chapter 2) is time-consuming due to the computer time required to perform digital autocorrelations of the image fields. Fast optical autocorrelations are possible using Fourier lenses and photorefractive materials: in this case the computer image processor need only read the location of the autocorrelation peaks stored in the photorefractive crystal rather than compute the digital autocorrelation (Buchhave and Jakobsen, 1990; Marrakchi et al., 1991). Such an increase in analysis speed would make PIV much more useful for flow measurements, especially those with transient conditions and/or a large test matrix.

A photorefractive PIV (PPIV) system had been proposed for investigation as part of this program. However, due to the image degradation limits cited in the previous sections, this portion of the work was not attempted.

4.5 Summary

$BaTiO_3$ has been demonstrated as a significant visualizer of turbulent vs. steady-state flow. However, we have identified two potentially significant limitations in that it (1) appears to visualize gradients differently, depending upon the relative orientation of the gradient to the crystal fanning orientation, and (2) visualizes refractive gradients, not absolute phase change, as reported in at least one reference. The desired quantification of photorefractive measurements proved to be very difficult for the reasons discussed above.

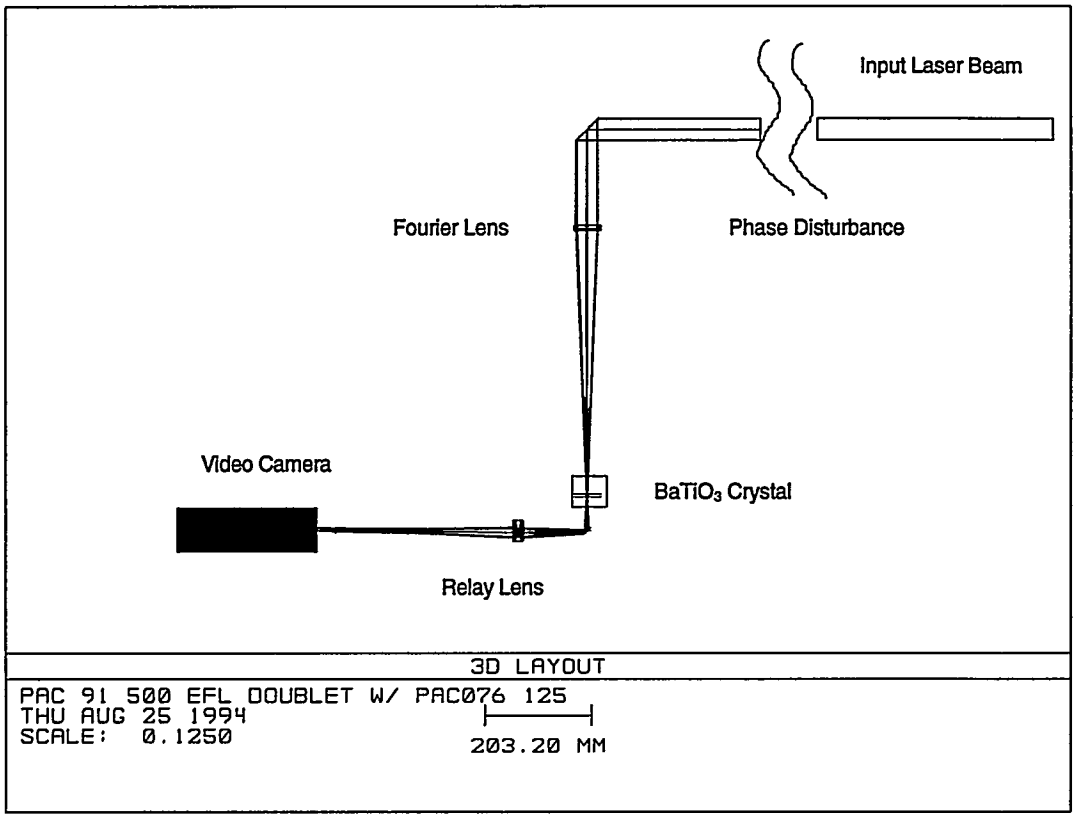

Figure 4.1. Schematic layout of optical system for power spectral density (PSD) measurements. Fourier lens 500 mm focal length, relay lens 125 mm focal length. Video camera images Fourier plane of relay lens.

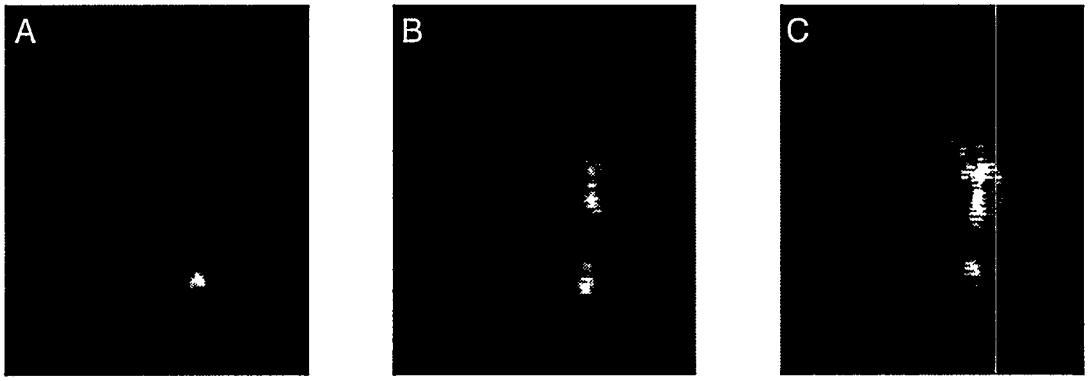

Figure 4.2. Turbulent power spectral density (PSD) measurements. (A) Static background image (no flow). (B) Gas jet: low-flow conditions. (C) Gas jet: high-flow conditions.

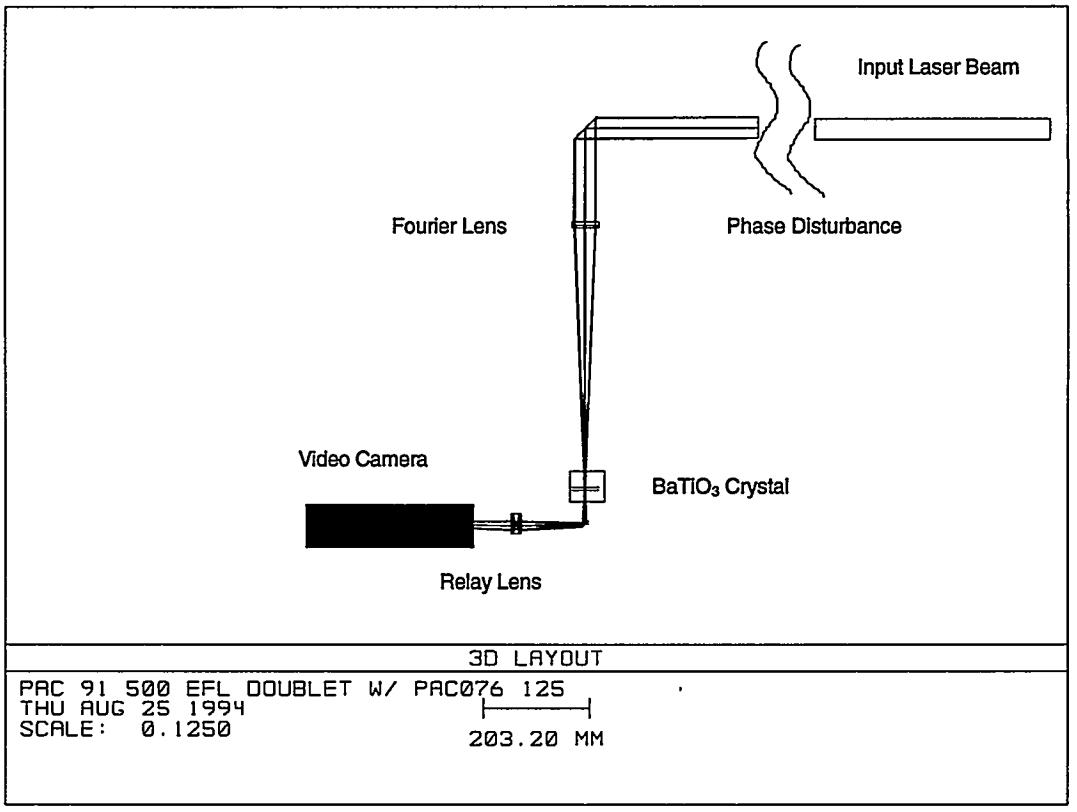

Figure 4.3. Schematic layout for photorefractive schlieren technique. Video camera images the phase disturbance plane.

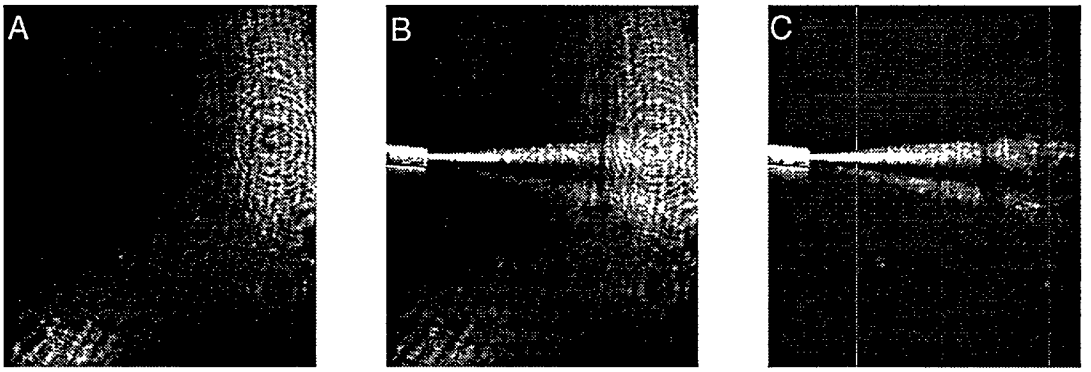

Figure 4.4. Photorefractive schlieren flow visualization with $BaTiO_3$. (A) Background field, no flow. (B) CO_2 jet flow field. (C) Jet flow field with background subtracted and image processed.

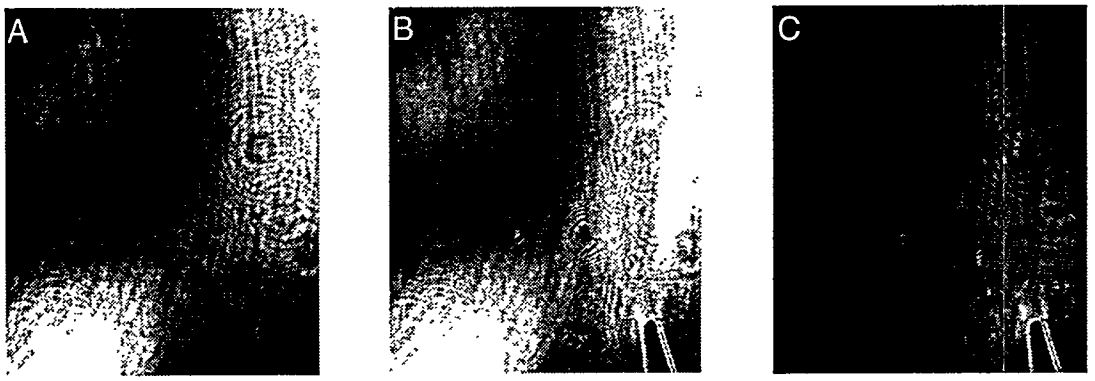

Figure 4.5. Effect of flow perturbation on $BaTiO_3$. Test object is hot soldering iron. (A) Static laminar flow. (B) Perturbed flow field (air currents). (C) Perturbed flow field with static flow subtracted.

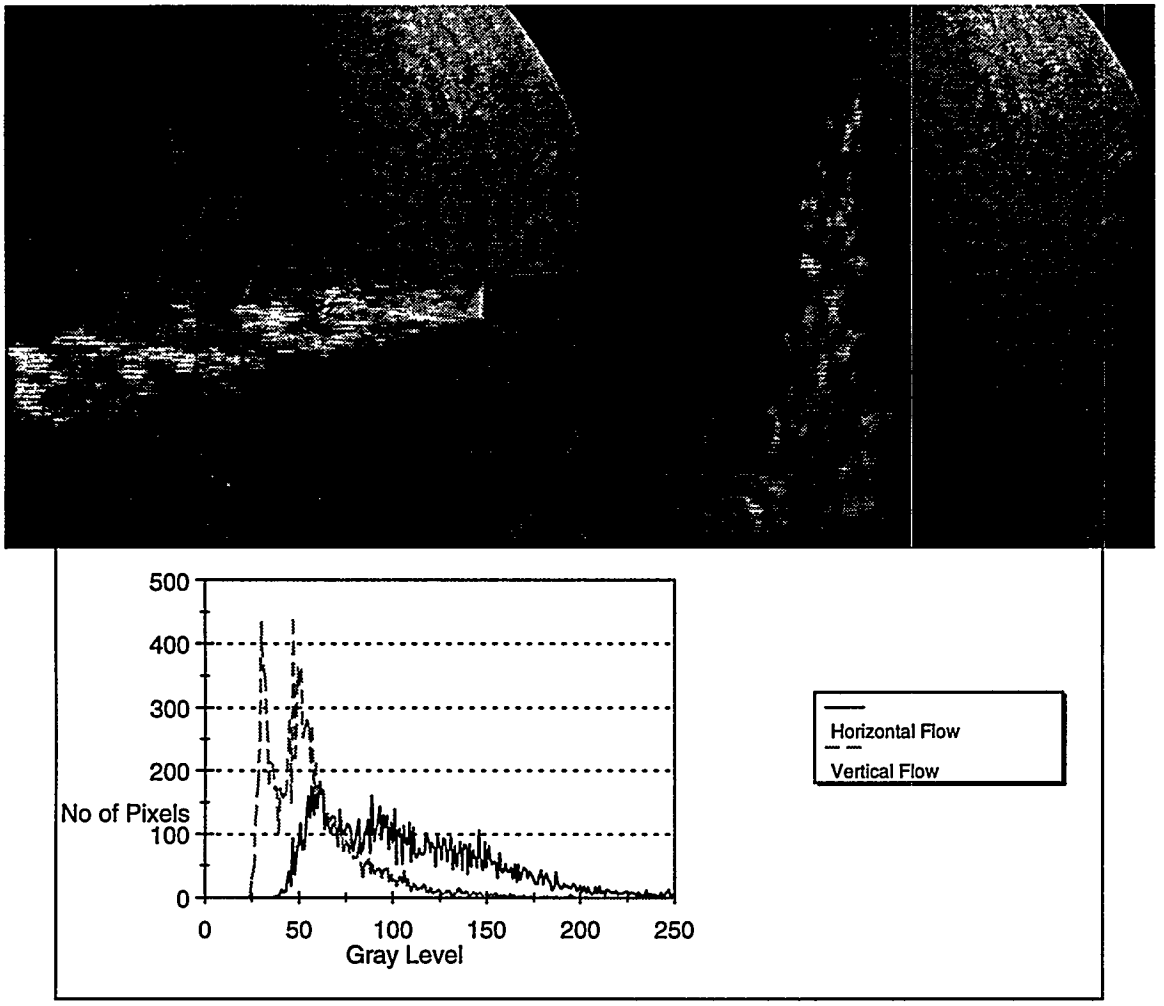

Figure 4.6. Orientation dependence of a turbulent CO_2 jet in air. (A) Horizontal flow. (B) Vertical flow. (C) Intensity histograms.

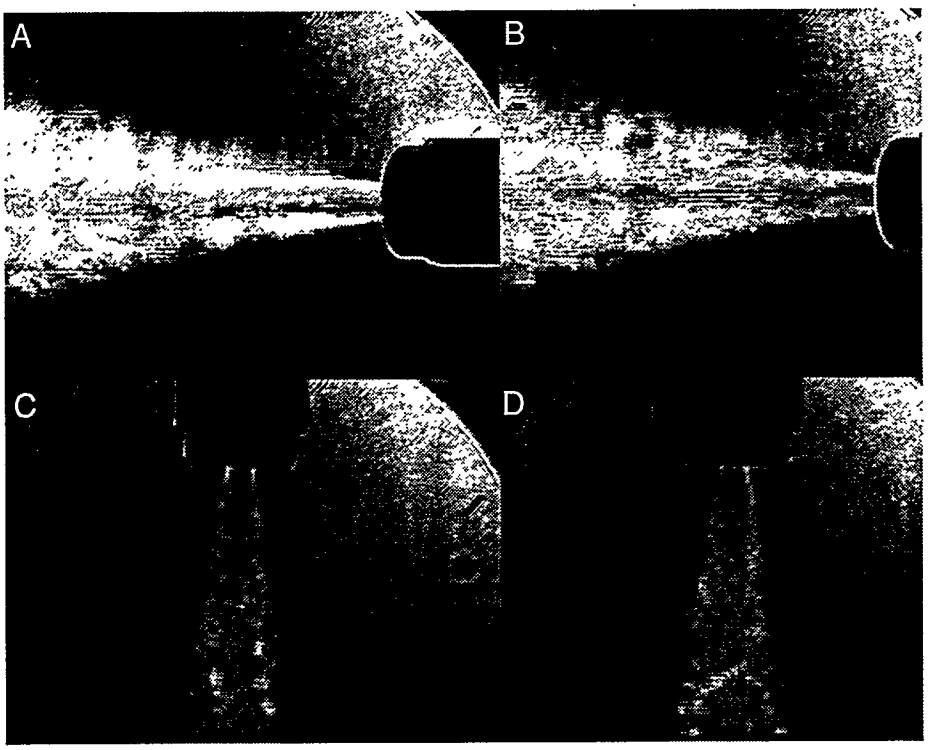

Figure 4.7. Dependence of photorefractive effect on gradient orientation. (A, B) Cross flow. (C, D) With flow. Crystal fanning is in vertical direction.

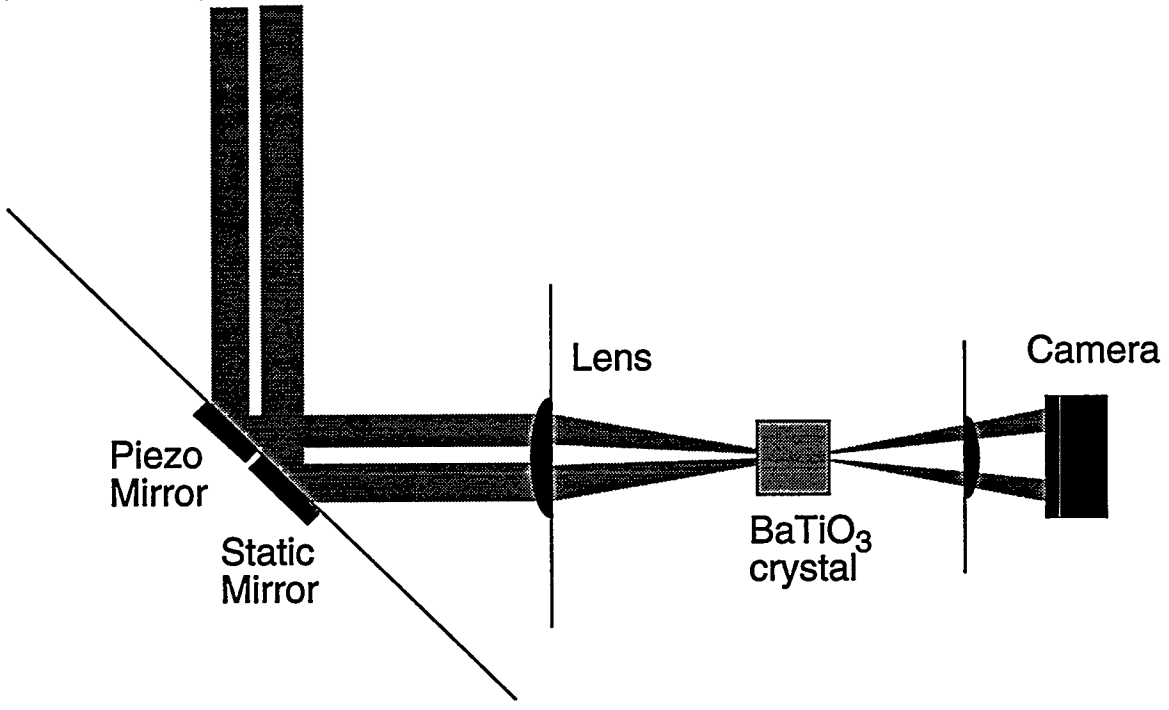

Figure 4.8. Schematic of phase sensitivity test setup.

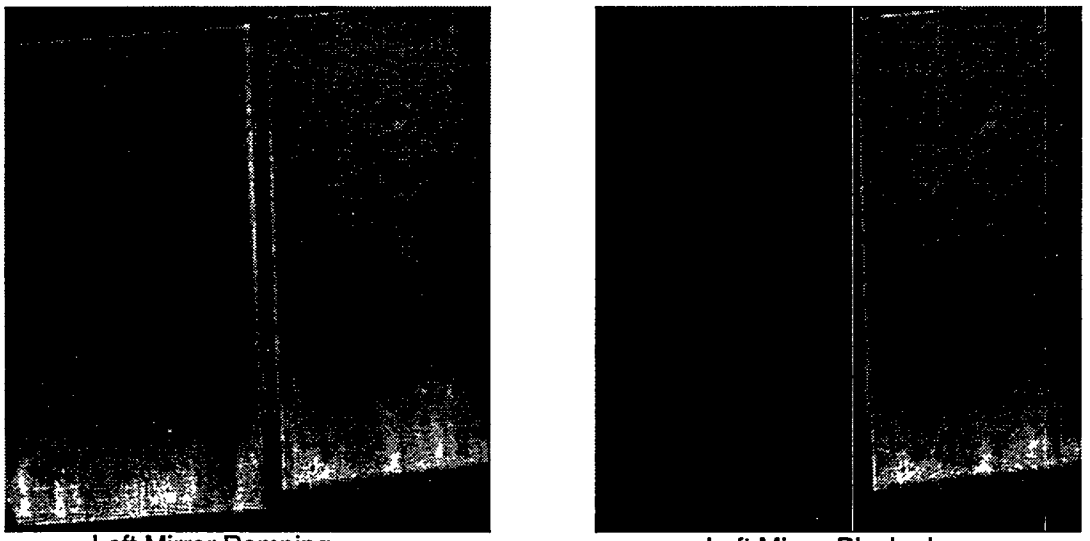

Figure 4.9. Phase shift test.

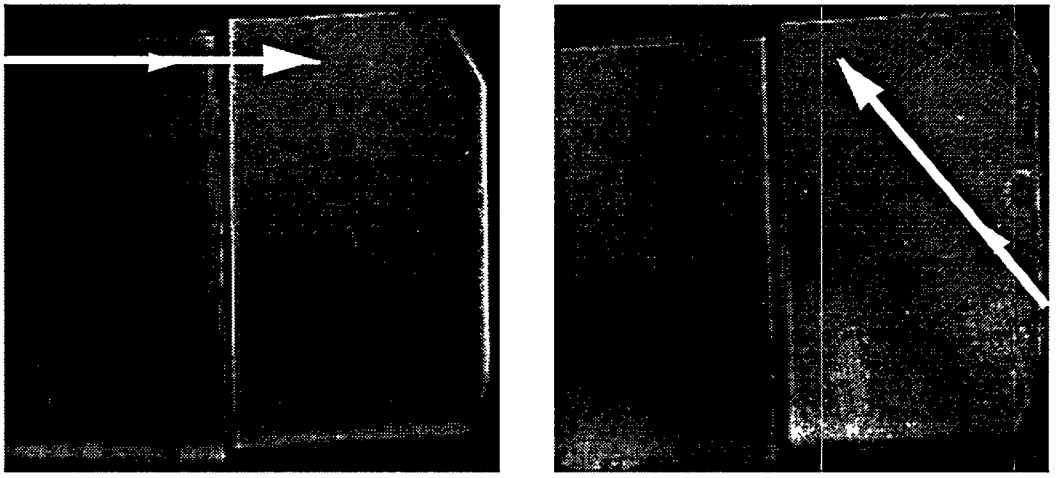

Figure 4.10. Effect of cross-coupling beams within crystal. The arrows point to regions of temporally modulated fringes.

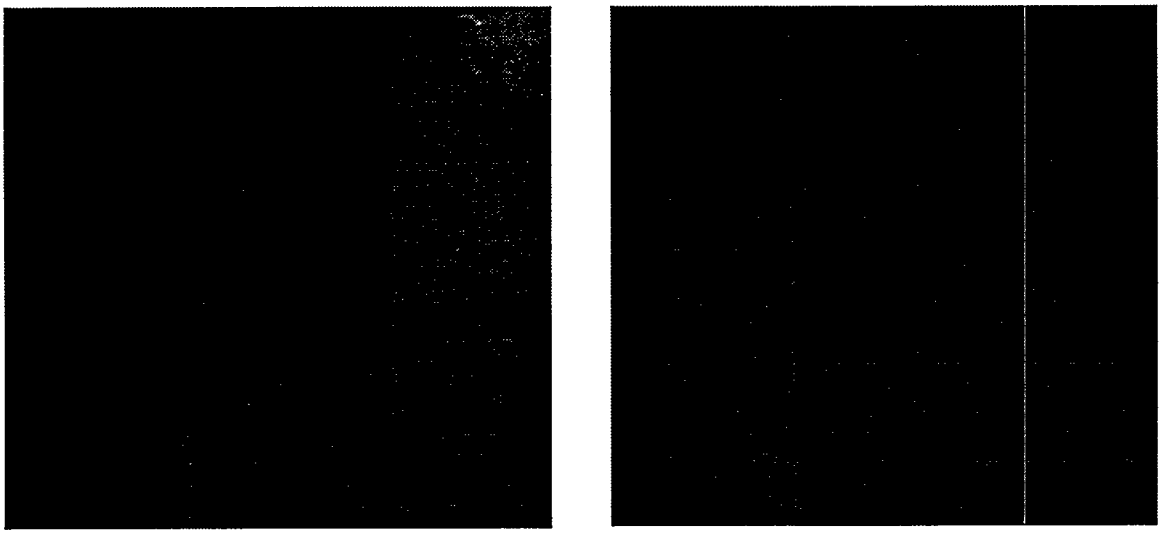

Vertical Strip Across Aperture Right 2/3 Aperture Blocked

Figure 4.11. Effect of a vertical aperture on wavefront extinction: fanning direction vertical.

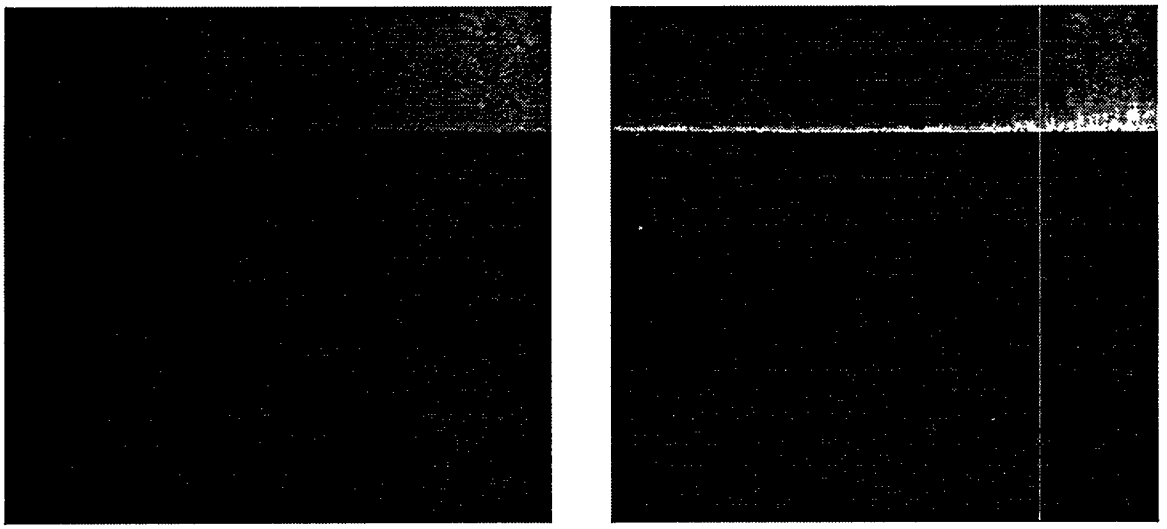

Narrow Strip Across Window Lower 2/3 blocked

Figure 4.12. Effect of a horizontal aperture on wavefront extinction: fanning direction vertical.

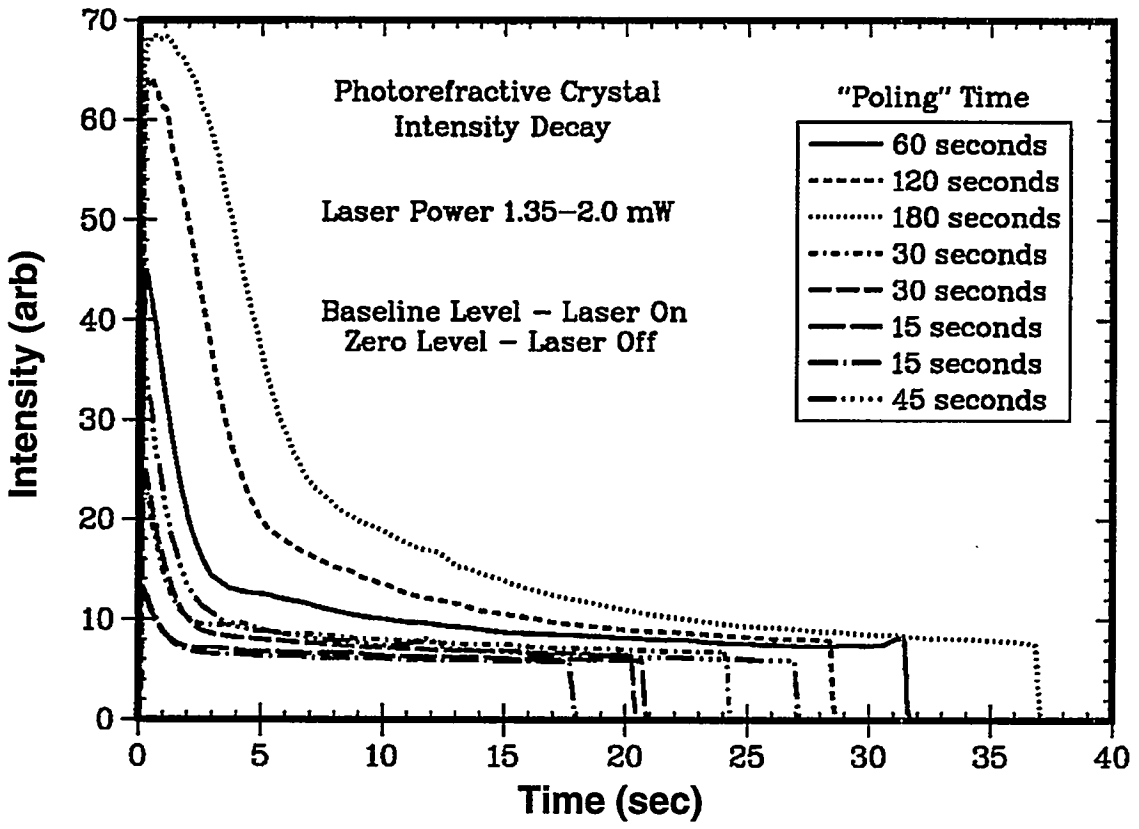

Figure 4.13. Crystal extinction vs. time for a variety of initial poling (erasure exposure) times. Incident laser power constant.

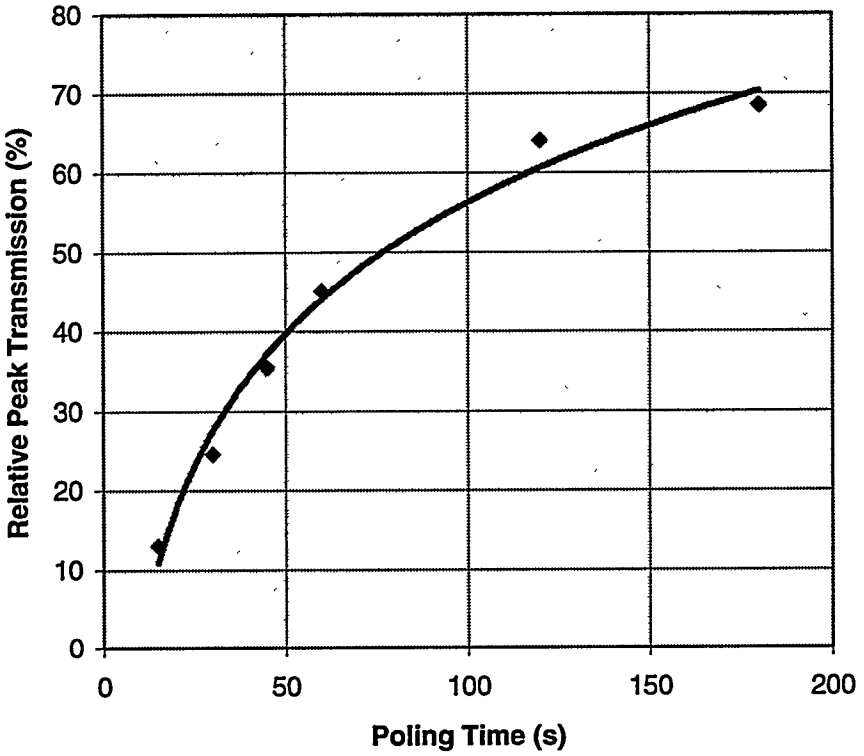

Figure 4.14. Crystal peak transmission vs. poling time.